Supporting Information

Unraveling the mechanism of the oxidation of glycerol to dicarboxylic acids over a sonochemically synthesized copper oxide catalyst

Prince N. Amaniampong, [a,#] Quang Thang Trinh,[b,#] Jithin John Varghese,[b] Ronan Behling,[c] Sabine Valange,[c] Samir H. Mushrif,[d,e*] Francois Jeromea,[c*]

[a] INCREASE (FR CNRS 3707), Université de Poitiers, ENSIP, 1 rue Marcel Doré, TSA41105, 86073 Poitiers Cedex 9, France

[b] Cambridge Centre for Advanced Research and Education in Singapore (CARES), Campus for Research Excellence and Technological Enterprise (CREATE), 1 Create Way, Singapore 138602, Singapore.

[c] Institut de Chimie des Milieux et Matériaux de Poitiers (IC2MP), Université de Poitiers,

[d] School of Chemical and Biomedical Engineering, Nanyang Technological University, 62 Nanyang Drive, Singapore 637459, Singapore.

[e] Department of Chemical and Materials Engineering, University of Alberta, 9211-116 St NW, Edmonton, Alberta T6G1H9, Canada.

Corresponding Author

* SHMushrif@ntu.edu.sg (SHM)

* francois.jerome@univ-poitiers.fr (FJ)

1. Experimental Methods

1.1. Preparation of Copper (II) Oxide Nanoleaves (CuO NLs) under ultrasound irradiation.

All chemical reagents were used without further purification. In a typical synthesis method, 40 mL of 0.25 M NaOH aqueous solution was added to 10 mL of 0.5 M $Cu(NO_3)_2$ aqueous solution and a sky-blue suspension was obtained. This suspension was subsequently exposed a low frequency ultrasound irradiation. Ultrasound was generated by a Digital Sonifier S-250D from Branson (power of standby P_o = 27.0 W, nominal electric power of the generator P_{elec} = 8.2 W). A 3.2 nm diameter tapered microtip probe operating at a frequency of 19.95 kHz was used. The volume acoustic power of this system was $P_{acous.vol}$ = 0.25 W.mL-1 in water (determined by calorimetry measurements)[1]. The ultrasound probe was immersed directly in the reaction medium and a Minichiller cooler (Huber) was used to control the reaction temperature at 25 ^oC. On completion of sonication at the desired time, the dark blue or black precipitates were washed thoroughly with distilled water and dried in an oven at 60 ^oC overnight.

1.2. Preparation of Copper (II) Oxide Nanoleaves (CuO NLs) under Mechanical stirring.

Copper (II) oxide nanoleaves synthesis procedure was adapted following the procedure previously described by Amaniampong *et al*.[2] Briefly, 20 mL of 0.25 M NaOH aqueous solution was added to 5 mL of 0.5 M $Cu(NO_3)_2$ aqueous solution under stirring at room temperature and the mixture was continuously stirred overnight. The solid sample was then washed with deionized water several times and dried in an oven at 60 ^oC.

1.3. Catalyst Characterization

Crystallographic analysis of the CuO NLs were performed by means of XRD measurements in 2Θ mode on a Bruker AXS D8 diffractometer with $Cu_{K\alpha}$ (λ = 0.154056 Å) radiation at 40 kV and 20 mA. XPS was performed on a Thermo Escalab 250 spectrometer. The binding energy was calibrated using C1s (284.6 eV) as a reference. The as-synthesized CuO nanoleaves morphology

was also studied by SEM (JEOL JSM 6700F field emission), TEM and HR-TEM (JEOL JEM-2100F). Surface area analysis was determined by nitrogen physisorption on a Micromeritics TrisStar apparatus. The specific area was calculated using the Brunauer-Emmett-Teller (BET) equation.

1.4. Activity test and analytical methods.

The general procedure for testing the catalytic oxidation of glycerol over CuO NLs catalyst in the presence of H_2O_2 is briefly described here. Typically, about 0.100 g of glycerol was charged into a 25 mL capacity round-bottom flask and an appropriate amount of CuO NLs catalyst (unless otherwise stated) added. To this, 2 equivalent H_2O_2 and 2 mL of DI water were added sequentially. The reaction mixture was heated in a temperature controlled oil bath and heated to desired reaction temperatures. Once the pre-set temperature of the oil bath is attained, stirring rate was set at 250 rpm and reaction proceeds until the desired reaction time. After the reaction, approximately 05 mL of the reaction liquid sample was taken and diluted and filtered before HPLC analysis. Oxalic acid, tartronic acid, glycolic acid, formic acid and glyceraldehyde were all confirmed using a Varian Pro Star HPLC equipped with an ICE-COREGEL 107H column 300 x 7.8 mm from Transgenomic, a UV/Vis detector (Varian Pro Star, 210 nm) and a refractive index detector (Varian 356-LC). A H_2SO_4 aqueous solution (7 mM) was used as the eluent with a 0.4 mL min^{-1} flow rate. External calibration of the liquid chromatography was performed using standards of oxalic acid, glycolic acid, glycerol, tartronic acid, glyceraldehyde and formic acid was quantified by the difference between the two HPLC analyses. Noteworthy, the detected amount of formic acid reported in our study is the solubilized fraction of it, although the volatized amount of formic acid at the analyze condition is small according to its corresponding Henry's law coefficient.[3] After each set of reaction, the catalyst is filtered off, by washing

thoroughly with DI water, it is then dried in an oven at 60 °C overnight. The recovered dried samples are weighed to estimate the exact amount of recovered catalyst after recycling. Typically, 90-85 % of the catalyst amounts are recovered. All other reactant amounts are adjusted to the amount of recovered catalyst in order to obtain uniform reaction parameters throughout the experiment.

2. N_2 adsorption-desorption isotherm of the synthesized CuO NLs

The nitrogen adsorption-desorption of the CuO NLs (Figure S1) revealed a type II isotherm with a type H_3 hysteresis loop. This is characteristic of the evolution of macroporous materials and the formation of plate-like particles, respectively, according to the IUPAC classification.

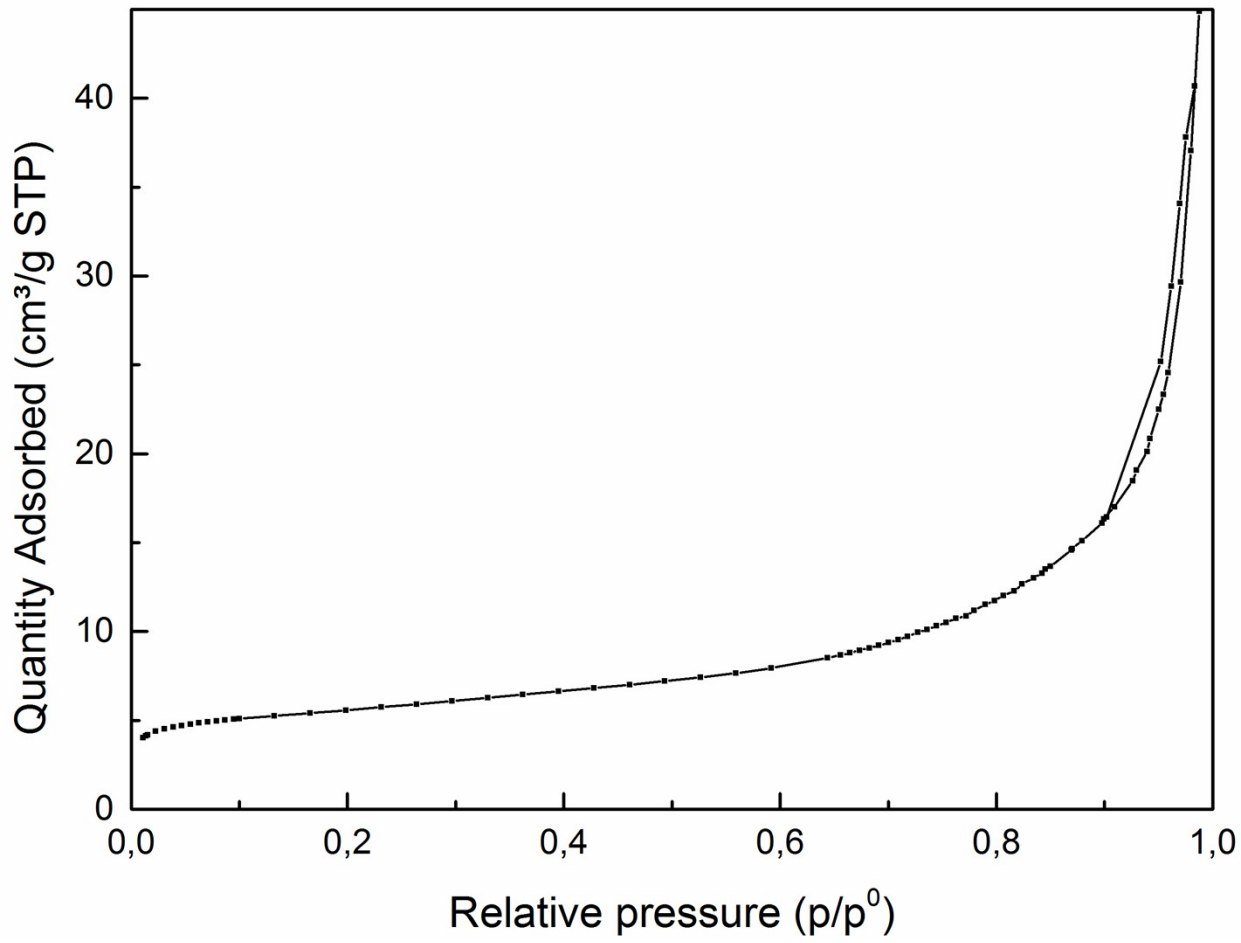

Figure S1. N_2 adsorption –desorption isotherm for the ultrasound synthesized CuO NLs

3. Cu LMM spectra analysis of the as-prepared CuO (US)

The Cu LMM spectra for the as-prepared CuO (US) catalyst was analyzed to further confirm the existence of CuO. The main peak position of Cu LMM for Cu at 918 was shifted to lower kinetic energy at 917.1 eV for the synthesized CuO catalyst. This value is strikingly similar to literature reported values of Cu LMM for CuO[4].

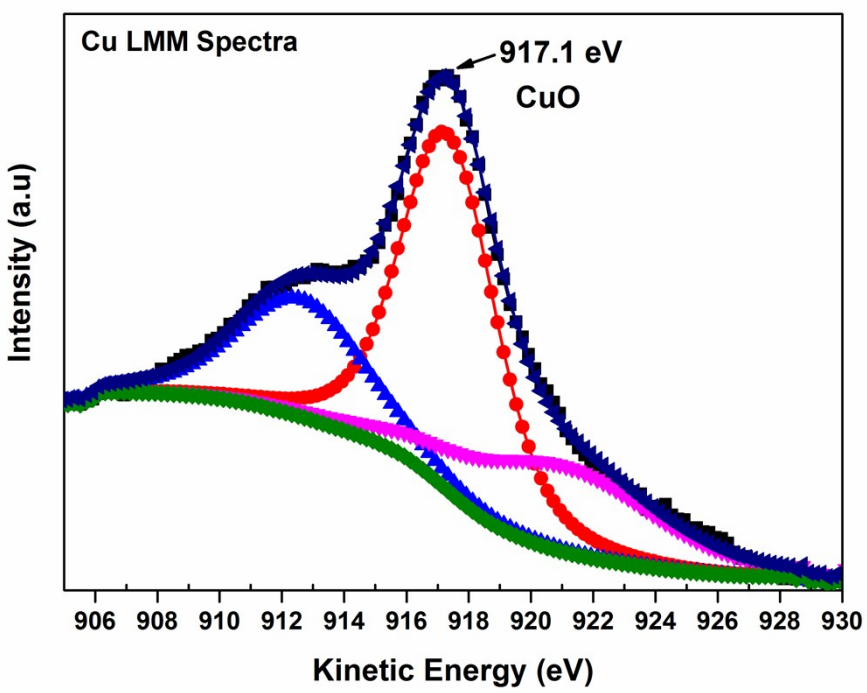

Figure S2. Cu LMM analysis of the as-prepared CuO (US)

4. XRD analysis of recovered CuO catalysts

XRD analysis was performed on samples recovered after the oxidation of glycerol in the absence of H_2O_2. The analysis results revealed a complete reduction of CuO to Cu_2O and Cu, indicating that in the absence of H_2O_2, lattice oxygen of CuO catalyst is consumed in the oxidation of glycerol. The XRD is shown in Figure S3.

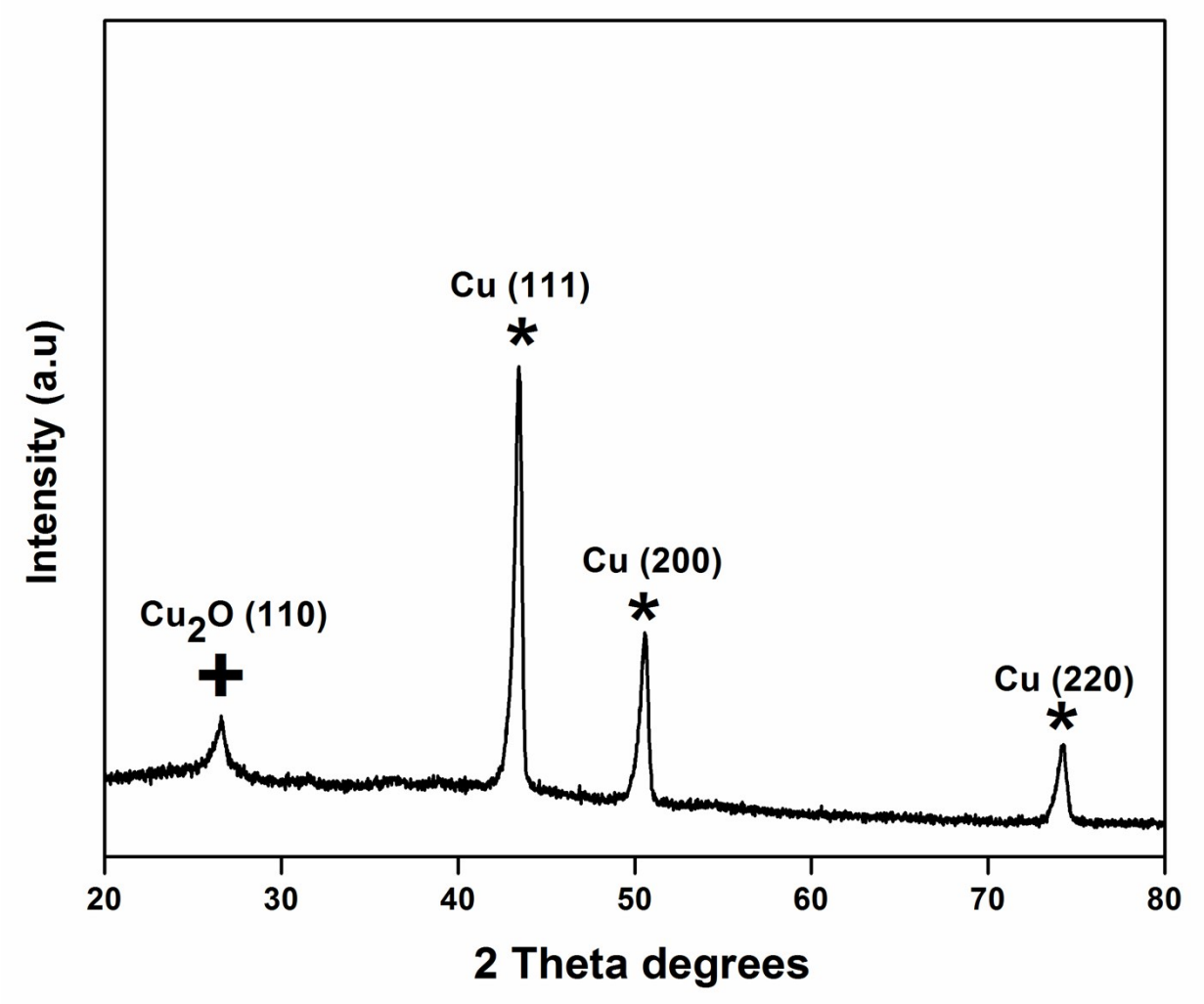

Figure S3. XRD analysis of recovered catalysts in the H_2O_2-free oxidation of glycerol

5. Isotope labeling experiment to confirm the source of oxygen

Glycerol oxidation reaction was performed in isotpe labeled H_2O_2 ($H_2{}^{18}O_2$), while keeping all other reaction conditions constant. After 4 hrs of reaction, final products were filtered and collected for ESI-MS analysis. Figure S4 shows the ESI-MS spectra of the analyzed product. A conspicrous peak (M/Z 91.04, [M-H^+]), which is attributed to ^{18}O-oxalic acid confirms that ^{18}O-oxygen (from H_2O_2) is present in the final dicarboxylic acid formed. A minor fragment observed at M/Z 89.02 [M-H^+] indicates the presence of normal ^{16}O-oxalic acid (relative molecular weight 90.03), but with a relatively lower intensity.

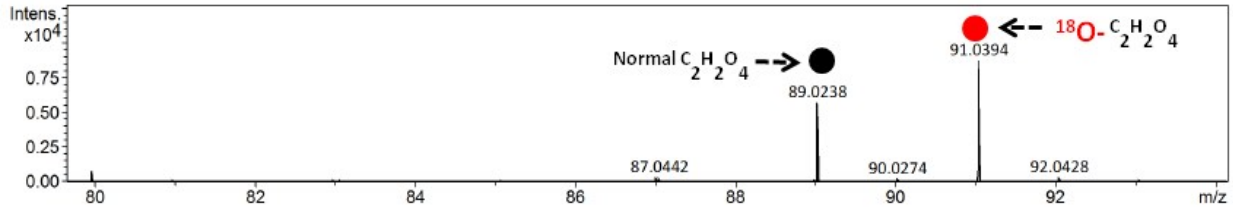

Figure S4. ESI-MS Spectra of the reaction performed in $H_2{}^{18}O_2$ labeled hydrogen peroxide

6. FT-IR analysis of recovered CuO catalyst after 4th recycling experiment

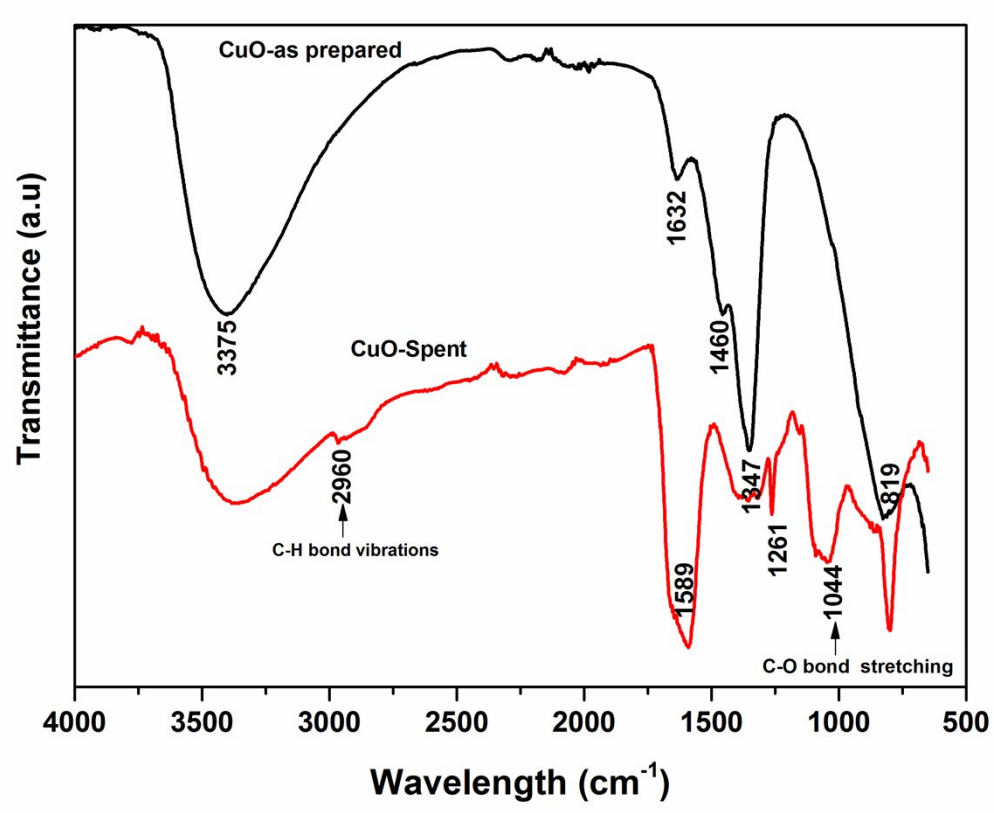

Figure S5. FT-IR analysis of recovered CuO catalyst

6. XRD analysis of recovered CuO (CM) and CuO (US) catalyst after 1st recycling experiment

XRD analysis of the recovered samples after the 1st recycling experiment revealed a mixture of Cu species in the form of Cu_2O, CuO and Cu.

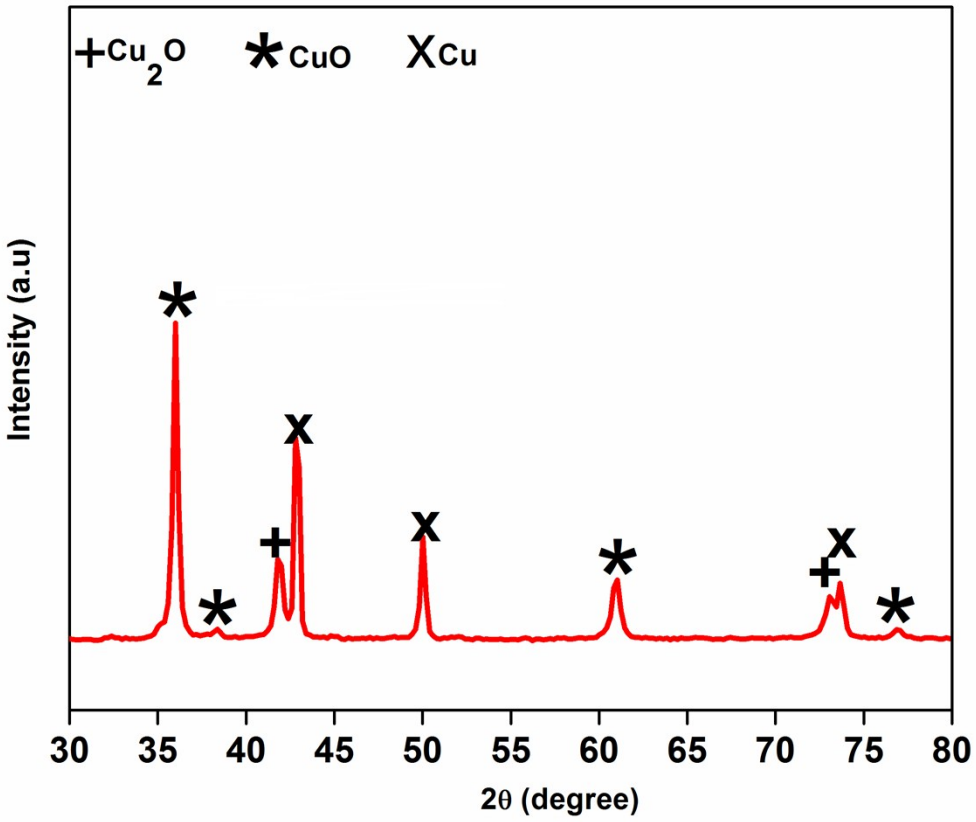

Figure S6a. XRD analysis of recovered CuO catalyst

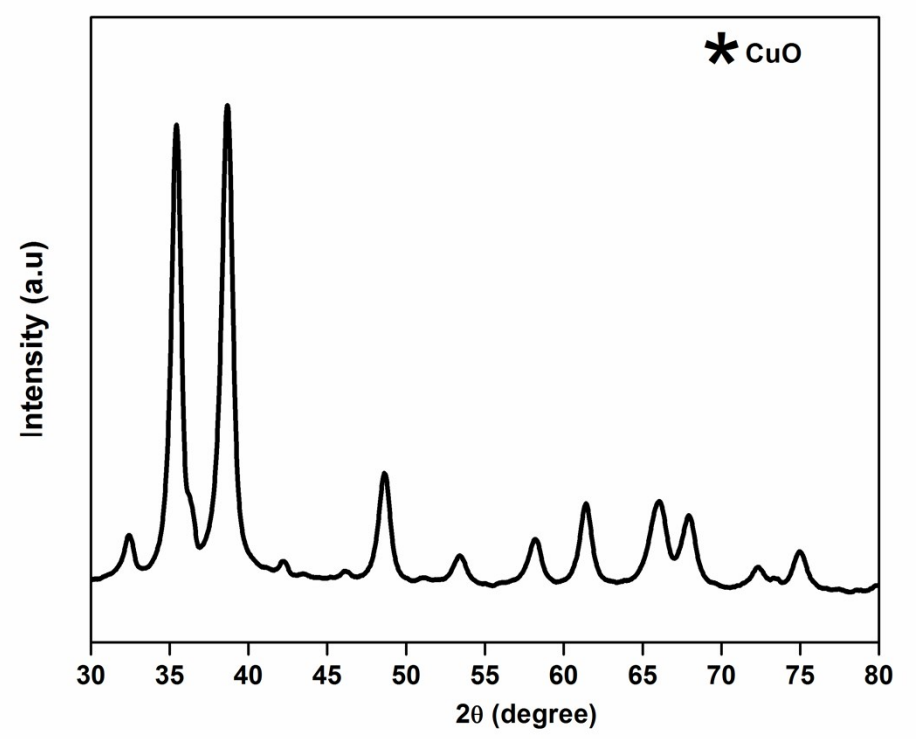

Figure S6b. XRD analysis of the recovered CuO (US) catalyst after 1st recycling experiment

7. Optimization of CuO-catalyzed oxidation of Glycerol

Initial catalytic experiments focused on the optimization of the reaction conditions. To this end, several reaction parameters were investigated such as reaction temperature, glycerol/H_2O_2 molar ratio and catalyst loading, the amounts of catalyst loading and the amount of oxidant on the yield of OXA and TAR were studied. The oxidative conversion of glycerol was first carried out over a range of temperatures (30-100 ^oC) as seen in **Figure S7**. As expected, a positive effect on the glycerol conversion was observed with an increase in temperature. More precisely, a sharp increase in conversion from 30 to 50 % was observed when the temperature was raised from 30 to 40 ^oC, respectively. A complete conversion (100 %) was achieved at 100 °C. The temperature profile investigations revealed that, once TAR was formed, it was relatively stable and does not undergo any significant degradation or oxidative decomposition. Conversely, the yield to OXA was observed to be ~ 9 % at 40 ^oC, which increased significantly with temperature and reached a maximum of 56 % at 80 ^oC. However, a sudden decreased in the yield to OXA was observed when the temperature was further increase from 80 to 100 ^oC (yield of 35 %). Hence, an optimum reaction temperature of 80 ^oC, based on the maximum yield to OXA and TAR was adopted throughout the investigation.

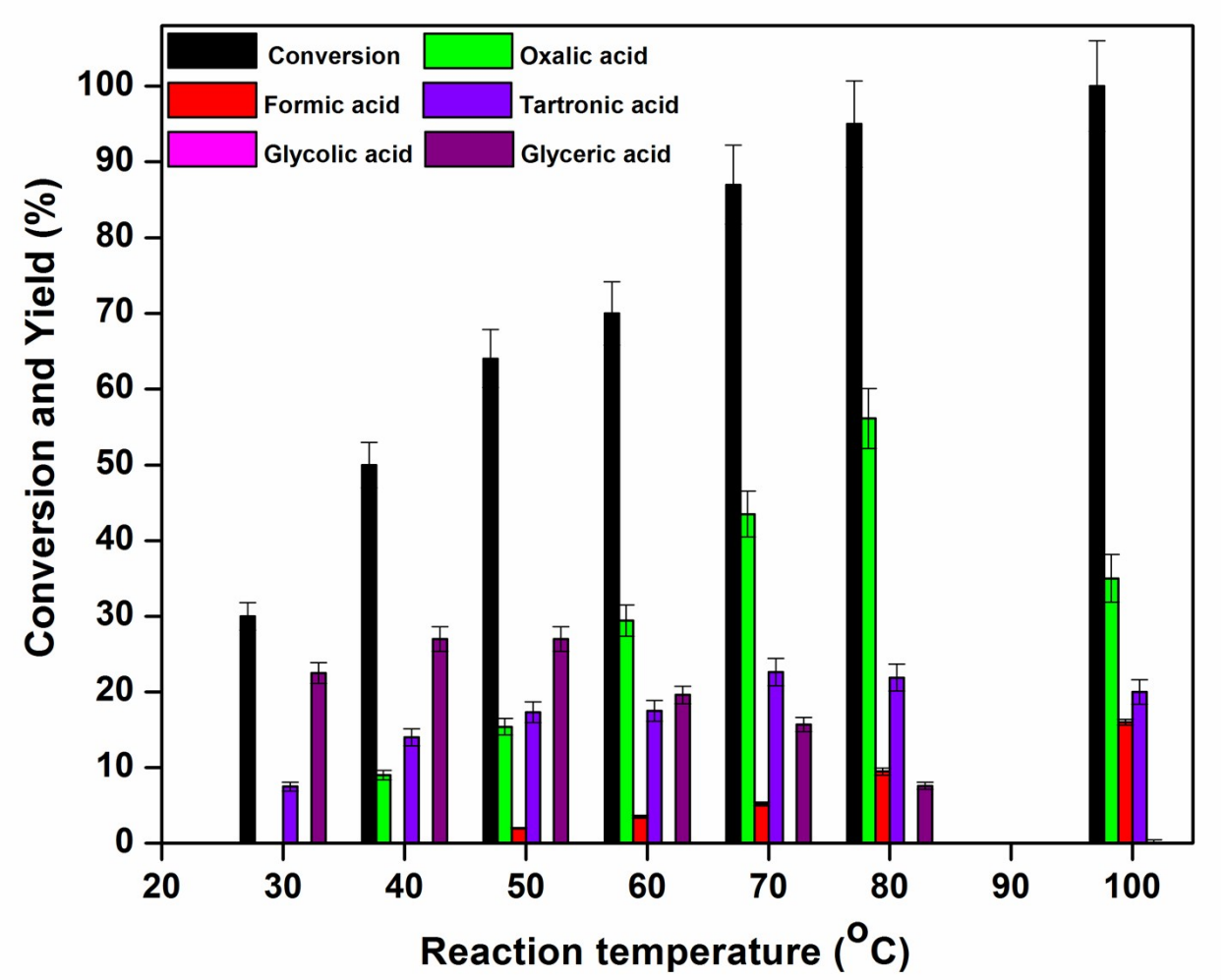

Figure S7. Effect of reaction temperature. Reaction conditions: 0.050g of CuO NLs, 0.100 g of glycerol, 2 eq. H_2O_2, 2 mL of H_2O, 4 h reaction time

More interestingly, we observed that of glyceric acid (yield 10 %) was formed in the presence of CuO catalyst without the addition of H_2O_2 (**Figure S8**). This can be explained by the fact that, reactions involving CuO and water can results in the formation of OH species via the cleavage of water molecules on the surfaces of CuO,[2] which in our experimental conditions could lead to the oxidation of glycerol. Note that formation of glyceric acid was not observed without CuO, further supporting this claim. A maximum yield to OXA and TAR of 56 and 22 %, respectively was observed at a glycerol/H_2O_2 molar ratio of 0.5. When the glycerol/H_2O_2 molar ratio was

increased to 1:3, the glycerol conversion reached 100% together with a yield to OXA and TAR of 50 % and 20%, respectively. However, a further increase in the glycerol/H_2O_2 to 1:3 and 1:4 led to a decrease of the carbon mass balance and a possible decarboxylation of formic acid and TAR to CO_2 and glycolic acid, respectively.

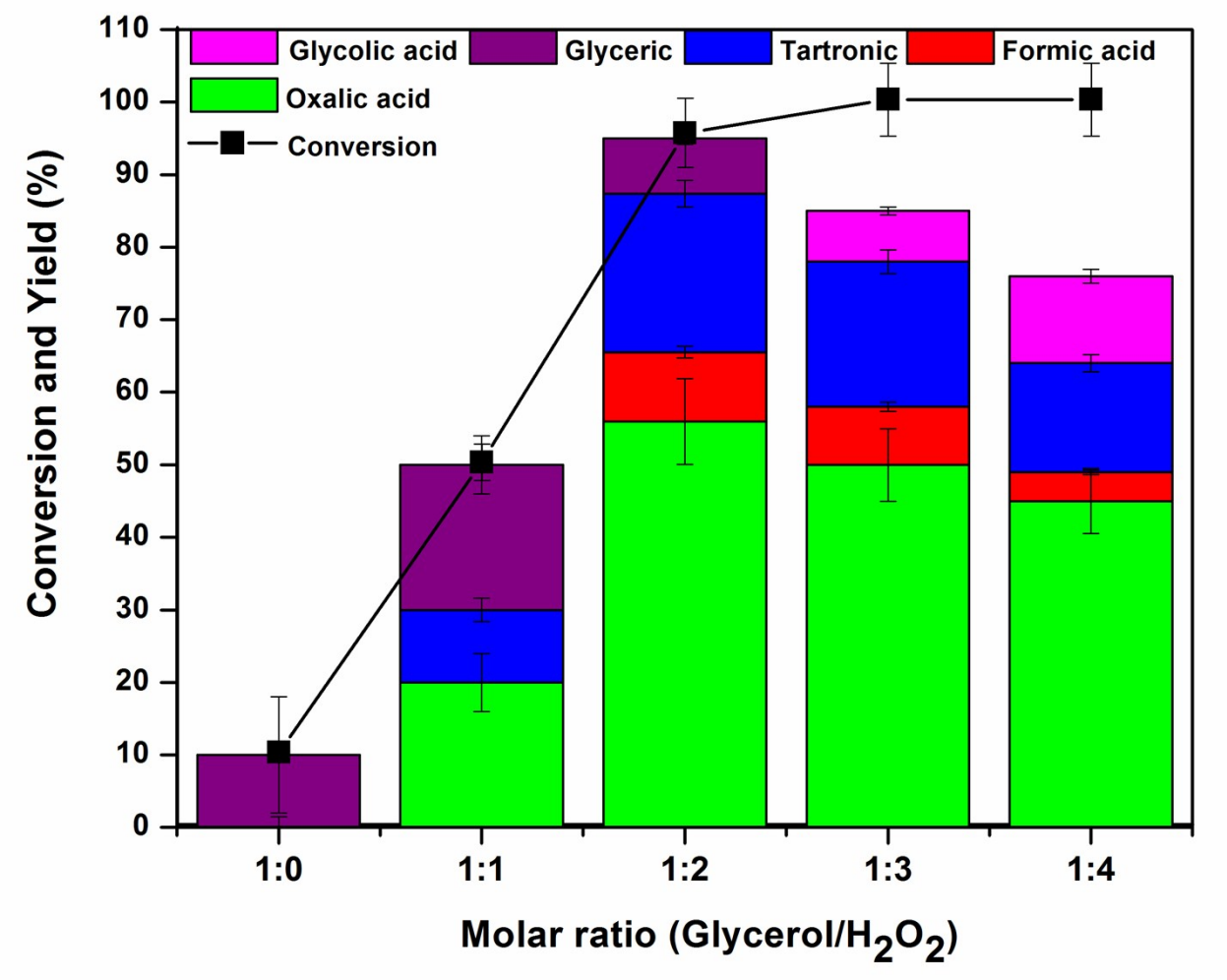

Figure S8. Effect glycerol/H_2O_2 molar ratio on the oxidation of glycerol. Reaction conditions: 0.05g of CuO NLs, 0.10 g of glycerol, 80°C reaction temperature, 2mL of H_2O, 4h reaction time

In the absence of CuO catalyst, no product was formed, though trace conversion of glycerol (< 2 %) was observed, probably due to the hydrothermal degradation of the substrate (**Figure S9**). The optimum catalyst loading was observed to be 20 wt. % of CuO related to the substrate.

Indeed, when higher amounts of catalyst were used in the reaction, a conversion increase was observed and quickly reaches a maximum (100 %) from 10 wt. % (60 % conversion) to 100 wt. % (100 % conversion). On the contrary, the yield towards OXA and TAR increased at 10 wt. % (22 and 10 %, respectively) to 20 wt. % (56 and 22 %, respectively), and further suffer from oxidative decomposition upon CuO amount increment in the reaction media.

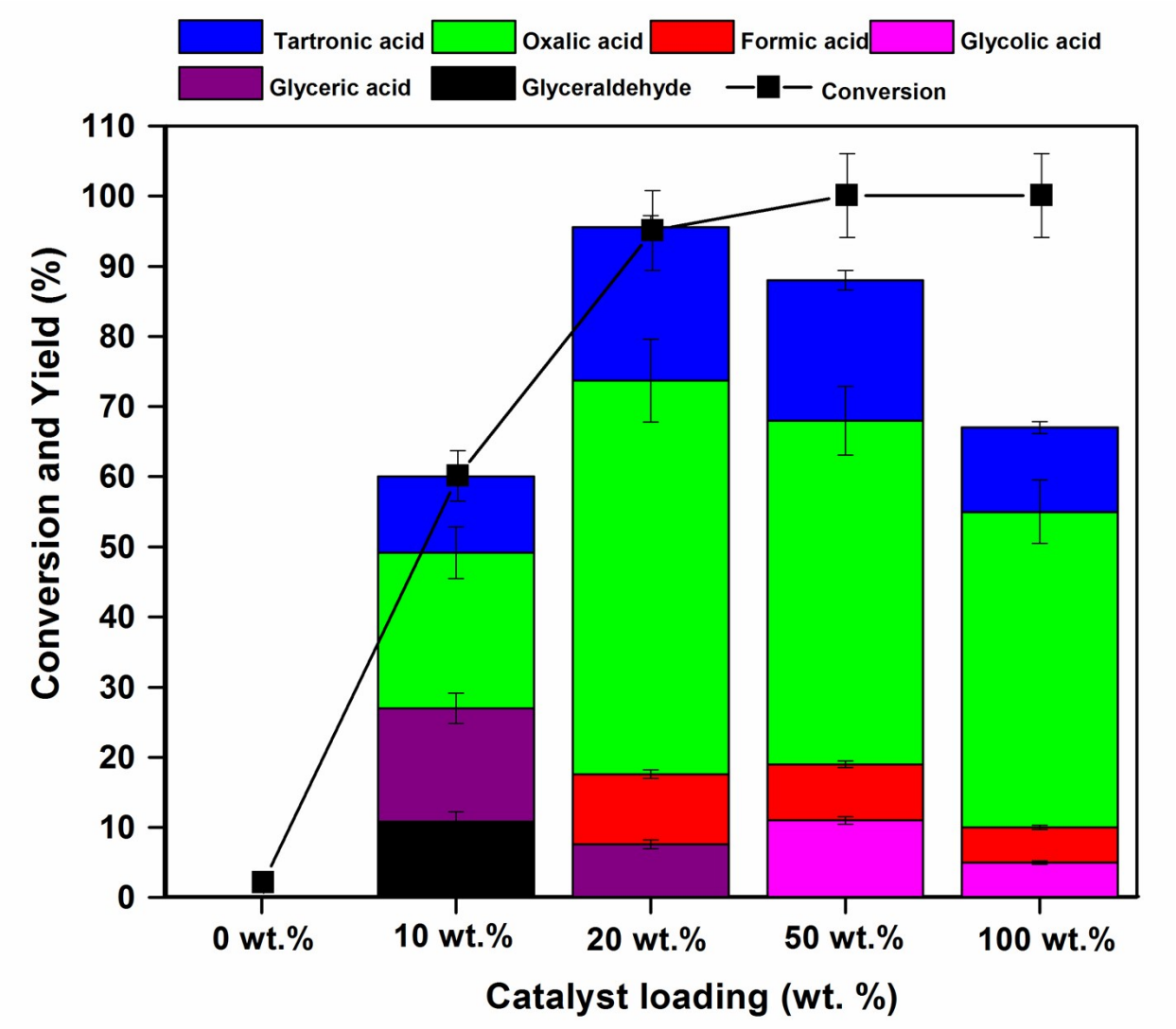

Figure S9. Effect of catalyst loading on the oxidation glycerol. Reaction conditions: 0.100 g of glycerol, 80 ^{o}C reaction temperature, 2 mL of H_2O, 4 h reaction time

Table S1. Comparison of the present work with the state of the art

Catalyst	Results			Conditions	Ref.
	Glycerol conversion (%)	Selectivity (%)			
		TAR	OXA		
CuO (Ultrasound synthesized)	**95.5**	**23**	**59**	**Glycerol (0.100g), 2 eq.H_2O_2, 80 °C, 4h, H_2O (2 mL)**	**This Work**
Cr(SO_3-salen)-CuMgAl-LDH	85.5	2.5	2.4	Glycerol (50mL);3% H2O2 (30mL);0.2g Catalyst, 60 ^oC, 6 h	3
Cr(SO_3-salen)-MnMgAl-LDH	41.5	11.5	0	Glycerol (50mL);3% H2O2 (30mL);0.2g Catalyst, 60 ^oC, 6 h	3
[Mn(SO_3-salphen)]- LDH	29.4	7.0	50.8	Glycerol (25mL);3% H2O2 (25mL);0.2g Catalyst, 60 ^oC, 4 h	4
Pt_{100}-starch/HT	88	13	12	Glycerol (0.5mmol) H_2O (2 mL); O_2 flow (10 $mLmin^{-1}$) 25 ^oC, 6h	5
AuPd/TiO_2 +$FeCl_3$	49	0	0.8	Glycerol/Au-Pd mole ratio (2500), 160 ^oC, 6h, O2 (1 MPa)	6
$Co_{0.15}$/Mg_3Al-s	100	63.5	24	0.5g Glycerol, 1.5g NaOH, 0.2g Catalyst, 70 ^oC, 24 h	7
AuPt/MgO	30	1	6	0.3M Glycerol, O_2 (3 atm), 80 ^oC	8
Au-Pd-Pt/TiO_2	100	14.8	2.2	Glycerol:NaOH =2:1, 60 ^oC, 4 h	9
2Au/CuO	16.4	0	4.6	0.1M Glycerol (20mL); O_2 (10 bar), 60 ^oC, 2 h	10
1Au/NiO	10.5	0	3.7	0.1M Glycerol (20mL); O_2 (10 bar), 60 ^oC, pH=6.7	10
1Au/NiO	19.6	30.6	5.0	0.1M Glycerol (20mL); O_2 (10 bar), 60 ^oC, pH=13.8	10
1Au/TiO_2	34.2	11.5	1.6	0.1M Glycerol (20mL); O_2 (10 bar), 60 ^oC, pH=13.8	10

8. Computational Methods

All the spin-polarized DFT calculations were done using the Vienna ab-initio simulation program (VASP).[5] Plane-wave basis set with a cut-off kinetic energy of 450 eV, the projector-augmented wave (PAW)[6] and the Perdew-Burke-Ernzerhof (PBE) functional[7] were utilized for those simulations. To correct the strong correlation and localization of 3d electrons of Cu in CuO structure, the Hubbard term in the form of GGA+U with U_{eff} = 7.0 ev was applied within the Dudarev's approach.[8] This correction described well the bulk properties (lattice parameters, band gap value and magnetic moment) of CuO and was successfully applied to simulate the activation of glucose and methane on CuO surfaces.[2, 9] In this study, CuO was modeled as periodic four-layer (4×2) slabs and a 20 Å vacuum thickness above the top layer was used to prevent interaction between repeated unit cells. Two top layers and the adsorbates were allowed to fully relax while the bottom two layers were fixed at the optimized bulk lattice parameters to reduce the computational cost without influencing the accuracy of simulations. Magnetic moment in the bulk-ordering is applied for CuO(111) surface since it was found to result in the most stable structure as reported by Mishra et al.[10] The 3×3×1 Monkhorst-Pack grid was used to sample the Brillouin zone, and the tetrahedron method with Blöchl corrections was employed for all calculations. Transition states were searched using the Nudged Elastic Band (NEB) method, and subsequently confirmed with the frequency calculations. To get the free energies of the process, the entropy, zero-point energy and enthalpy correction were computed from statistical thermodynamics for all adsorbed structures, while those values for gas-phase molecules were taken from the standard thermodynamics NIST-JANAF table.[11]

9. Adsorption of Glycerol on CuO(111) surface.

To evaluate the adsorption configuration of glycerol at different coverages, two scenarios were considered: the first corresponds to the configuration when only one glycerol molecule is adsorbed on CuO surface (called Scenario 1, representing low coverage), and the second corresponds to the configuration when two glycerol molecules are placed close to each other (called Scenario 2, to illustrate high coverages).

9.1. Scenario 1 – Adsorption at low coverage.

At low coverages, glycerol could adsorb on CuO surface via 4 different configurations: 1) bound to surface via its single primary OH (terminal OH) (Figure S10A), 2) bound to surface via its single secondary OH (Fig.S10B), 3) bound to surface via both primary and secondary OHs (Fig.S10C) and 4) bound to surface via both the primary OHs (terminal OH) (Fig.S7D). The stability is in the order B < A < C < D. In the most stable adsorption configuration (Fig.S7D), the adsorption energy is -104 kJ/mol.

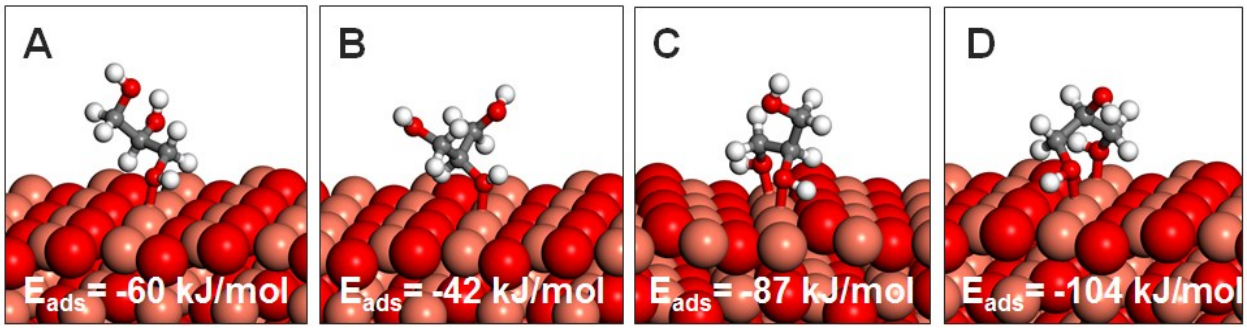

Figure S10. Adsorption configurations of glycerol on CuO(111) surface at low coverages. A) glycerol bound to CuO surface via its single primary OH; B) glycerol bound to CuO surface via its single secondary OH ; C) glycerol bound to CuO surface via one primary and one secondary OH; D) glycerol bound to CuO surface via both primary OHs.

9.2. Scenario 2 – Adsorption at high coverages.

To make the comparison more convenient, both, the average binding energy E^{ads}_{avg} and the differential binding energy E^{ads}_{diff}, are computed and the adsorption structure of glycerol at high coverages is presented in Figure S8. Only configurations in Figs. S10A and S10D are evaluated here (other configurations are even less stable at higher coverages due to the geometrical constraint). At higher coverages, adsorption configuration of glycerol in Fig. S10D is not the most stable configuration anymore. Due to the geometrical constraint, the energy gain E^{ads}_{diff} for adding one more molecule of glycerol next to the existing one in the configuration in Fig. S10D (coordination via both primary OHs) is only -32 kJ/mol and the average binding energy E^{ads}_{avg} is reduced from -104 kJ/mol (Fig.S10D) to only -67 kJ/mol (Fig.S11A). On the contrary, adding one more molecule of glycerol next to the existing one in configuration in Fig. S10A (coordination via only one primary OH) is much more preferred with the differential binding energy E^{ads}_{diff} of -99 kJ/mol (Fig.S11B) due to the inter H-bonding stabilization between adjacent glycerol molecules, making it the most stable configuration with the average binding energy E^{ads}_{avg} of -81 kJ/mol. Therefore, we choose the adsorption configuration of glycerol on CuO(111) surface where it coordinates to CuO surface via only one primary OH group (configuration S10A) to build the reaction energy for glycerol oxidation to glyceric acid in Figure 5 of the main text. This configuration is also widely used for DFT simulations on glycerol oxidation over transition metals surface in the literature.[2, 12] It is worth mentioning that even using the adsorption configuration in Fig. S10D (coordination via both two primary OHs), the activation barriers for the initial primary OH activation (43 kJ/mol, Fig. S9a) and subsequent CH activation (59 kJ/mol, Fig.S12b) are almost identical to the barriers using adsorption configuration in Fig. S10A (49 kJ/mol and 63 kJ/mol for the initial OH and subsequent CH

activations, respectively). After glyceraldehyde is formed, it prefers adsorption in the di-σ configuration and coordinates with the surface via only its formyl functional group (Fig.S11c) which is the most stable configuration and consistent with earlier studies.[2, 12b]

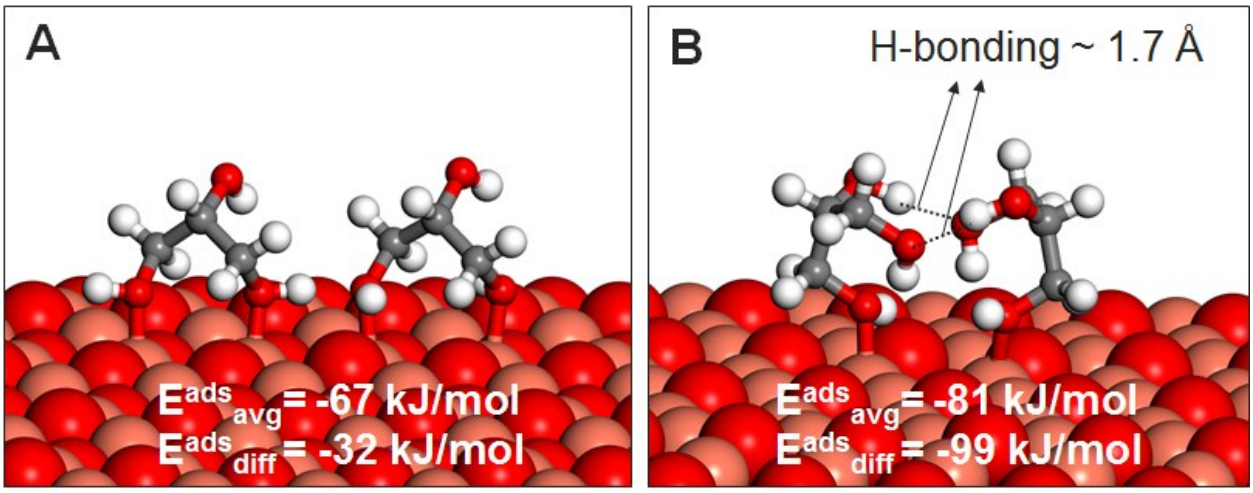

Figure S10. Adsorption configurations of glycerol on CuO(111) surface at high coverage. A) two glycerol molecules coordinating via two primary OHs; B) two glycerol molecules both coordinating only via the single primary OH. H-bonding is indicated by dash line.

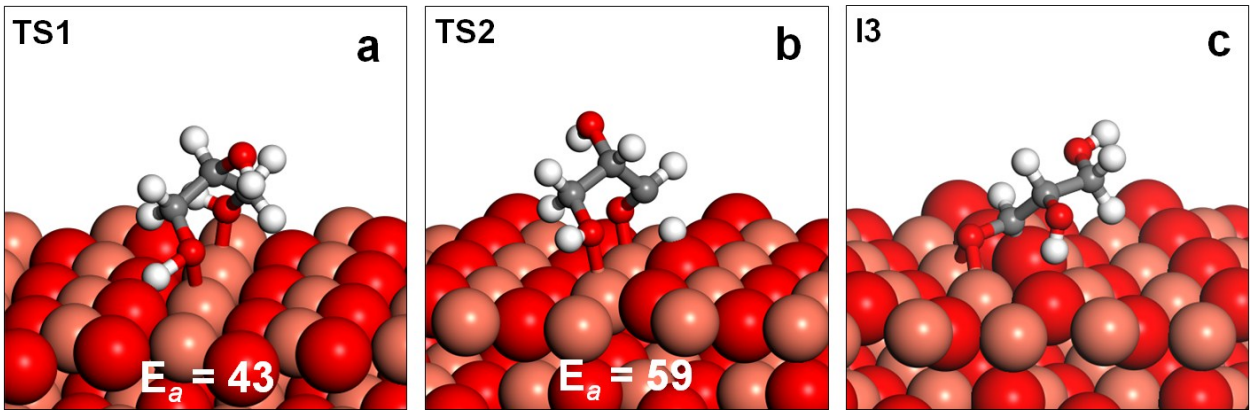

Figure S11. Activation of glycerol using adsorption configuration in Fig. S9. A) Initial primary OH activation; B) subsequent CH activation forming glyceraldehyde; C) most stable adsorption configuration of glyceraldehyde (intermediate I3 in Fig.5a of main text)

10. Initial C-H activation of glycerol on the clean CuO(111) surface:

Instead of the lowest initial OH activation pathway with the activation barrier of 49 kJ/mol as shown in Fig.5b in the main text, glycerol could undergo an initial C-H activation. The C-H bond can be activated only by the surface Cu_3 site with activation barrier of 297 kJ/mol (Fig. S12A), or via the "4-center mechanism" synergistically by both Cu_3 and O_3 site[9b] with a lower activation barrier of 130 kJ/mol (Fig.S12B). However, all the C-H activation pathways have much higher activation barriers and are therefore unlikely to be preferred.

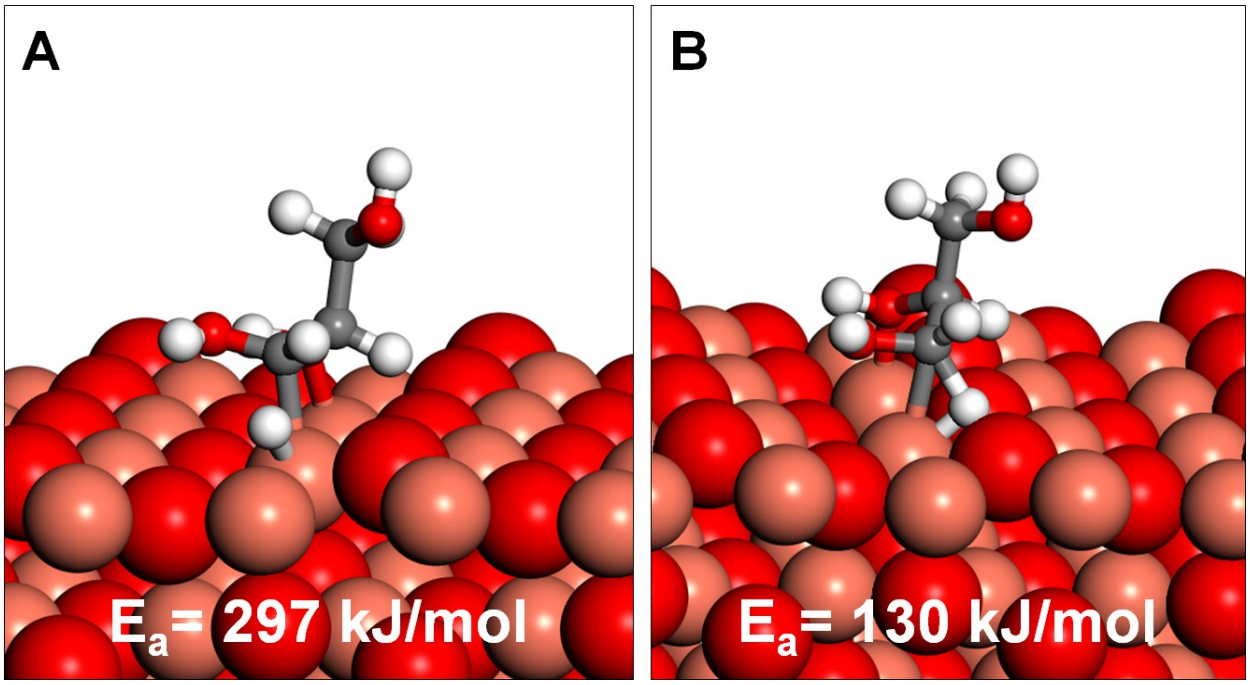

Figure S12. Initial C-H bond activation by A) only surface Cu_3 site and B) both surface Cu_3 and O_3 site via the "4-center mechanism"

11. Adsorption configuration of glyceric acid

After glyceric acid is formed from the protonation of glycerate by surface H (Fig.5g of the main text), it reorients on the surface to a more stable adsorption configuration and adsorbs on the surface via its primary OH which is 16 kJ/mol more stable (Figure S13). The oxidation of the other primary CH_2OH group in glycerol would proceed via the same mechanism for glycerol oxidation to glyceric acid, resulting in the formation of tartronic acid (TAR).

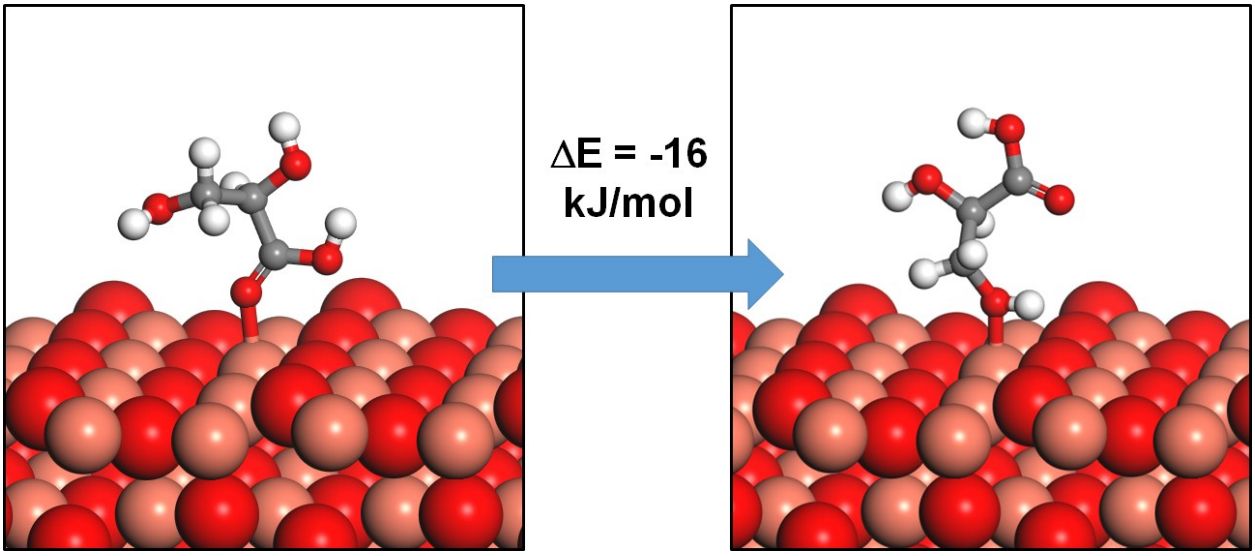

Figure S13. Reorientation of adsorbed glyceric acid

12. C-C cleavages

For the formation of OXA, the C-C cleavage has to occur. DFT calculations were performed to identify the precursors for the C-C cleavage and the results are shown in Figure S14 below.

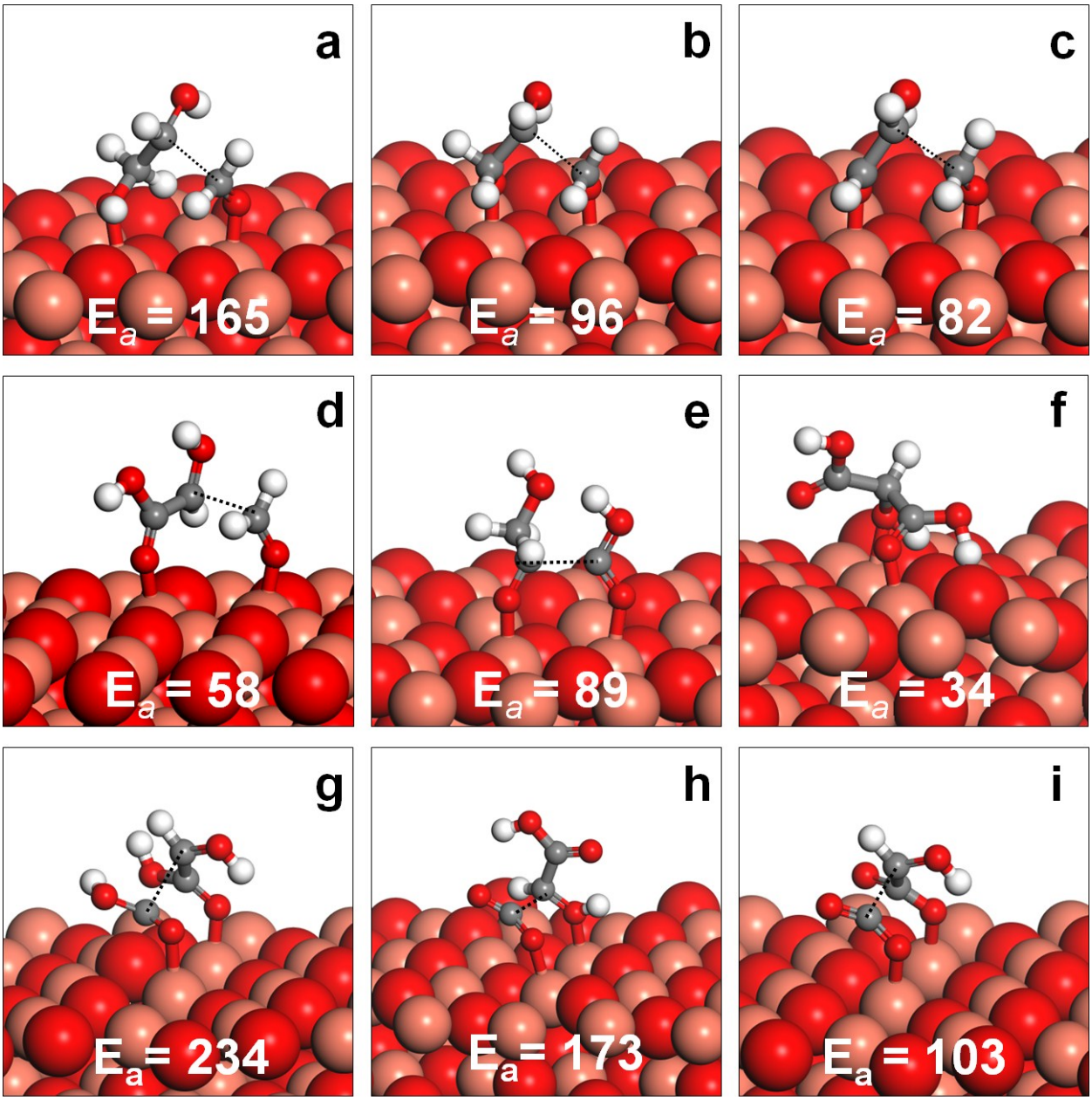

Figure S14. Transition states and activation barriers for C-C cleavages from different precursors.

The activation barrier for C-C dissociation in glycerol is very high (> 250 kJ/mol, not shown here). However after the activation of one of the primary OH of glycerol (which is very feasible with barrier of only 49 kJ/mol, Fig.5b in main text), the activation barrier for the C-C cleavage is reduced to 165 kJ/mol (Fig.S12a), inferring that the OH deprotonation would be the precursor for the C-C cleavage. To test this argument, we computed the barrier for C-C cleavage after both the terminal OH groups of glycerol are deprotonated. Indeed, the C-C dissociation barrier in that structure is 96 kJ/mol (Fig.S14b). These results suggest that the precursors for the C-C cleavage are structures which adsorb on CuO surface via both the terminal (1,3) oxygen atoms. This assumption is again validated for the C-C cleavage in deprotonated glyceraldehyde (route 1 in Scheme 1 of the main text) with the activation barrier of only 82 kJ/mol (Fig.S14c and Fig.7a in the main text). For glyceric acid route (Route 2, Scheme 1), the deprotonation of OH group is also the precursor for the C-C cleavage. However, the C-C cleavage from precursor which adsorb on CuO surface via both the terminal (1,3) oxygen atoms (58 kJ/mol, Fig.14d and Fig.S7b in the main text) is easier than in the precursor which adsorbs on CuO surface via one primary and once secondary (1,2) oxygen atoms (89 kJ/mol, Fig.14e).

Along the tartronic acid route (Route 3, Scheme 1), the above trend is also the same, but the barriers are higher than the barriers in Route 1 and 2. Indeed, the barrier for decarboxylation reaction in tartronic acid is very high (234 kJ/mol, Fig.14g). The deprotonation of the carboxyl group can be done with the barrier of 34 kJ/mol (Fig.S124) and after one carboxylic acid has been deprotonated, the barrier for C-C cleavage is lowered to 173 kJ/mol (Fig.S124). If both carboxylic acid groups are deprotonated, the barrier is further reduced to 103 kJ/mol (Fig.S124 and Fig.7c in the main text).

13. The formation of adsorbed OH on CuO(111) surface and reaction between surface OH with H atom to regenerate the blocked surface lattice O_3 active site

In the presence of H_2O_2, surface OH could be formed on the CuO surface and adsorbs on the bridge site between two adjacent Cu_3 sites (Figure S15a) via the reaction:

$$H_2O_2 + * \rightarrow 2OH* \qquad (1)$$

We have calculated the Gibbs free energy ΔG of reaction (1) at reaction conditions (T=80°C) via the equation: $\Delta G = \Delta E + \Delta H_{correction} + \Delta ZPE - T\Delta S$

whereas E is the DFT computed electronic energy, thermodynamic properties including entropy (S), enthalpy correction ($H_{correction}$), zero point energy (ZPE) of different adsorbed configurations were calculated from statistical thermodynamics for clean surface (*) and adsorbed OH (OH*) and were obtained from the standard thermodynamics NIST-JANAF table and corrected at specified reaction temperatures for gas phase H_2O_2.

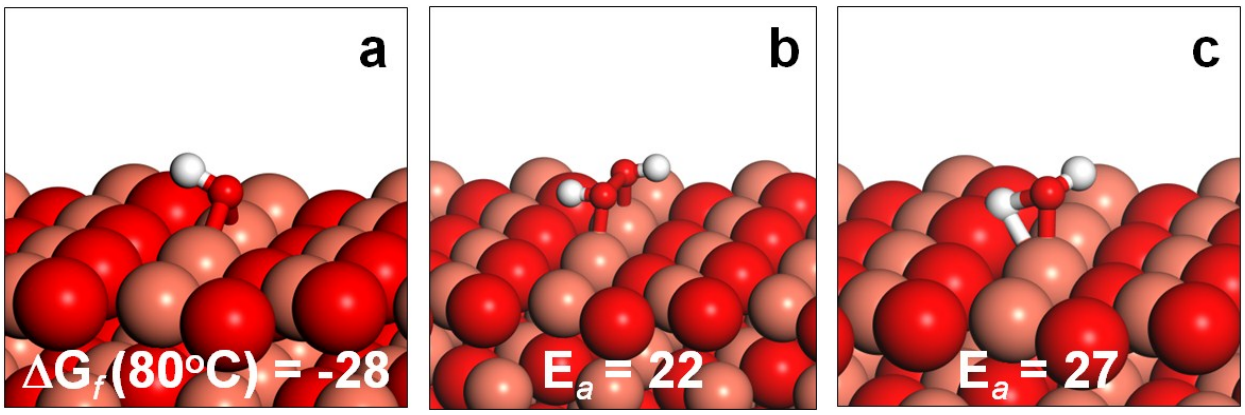

Figure S15. a) Adsorbed surface OH on CuO(111); b) Transition state of H_2O_2 activation; c) Transition state for the reaction between surface OH and H atom blocking surface O_3 site.

At 80°C, the free energy for the formation of surface OH is -28 kJ/mol (Fig.15a). Besides, the breaking of O-O bond in H_2O_2 to give two fragments of surface OH is also kinetically feasible

with the barrier of 22 kJ/mol only (Fig.15b). Therefore, the formation of surface OH species is both thermodynamically and kinetically favorable. As was mentioned in the main text, during the reaction, H atoms that are strongly bound on the active O_3 site will block those sites and reduce the activity of CuO. Surface OH can react with that H atom occupying the active surface O_3 site easily with the barrier of 27 kJ/mol (Fig.15c) via the reaction: $OH^* + H^* \rightarrow H_2O^* + *$. Due to this role of surface OH, the active O_3 site is regenerated and contribute into the high conversion of glycerol, as was observed experimentally in the main text.

14. Activation of glycerol assisted by surface OH on CuO(111)

Surface OH could also facilitate the C-H bond activation after the initial primary OH activation with the barrier of 67 kJ/mol (Figure S16a), as was shown in Fig.6 of the main text. Although this value is slightly higher than the barrier for the activation by surface lattice O3 site (Fig.5c), it involves the "on-the-fly" transfer of hydrogen from glycerol to the surface OH (TS5, Fig.6), and avoids generating the strongly bound H on the active O_3 site. Surface OH also assists in the H-abstraction form the complex after the insertion of surface OH into glyceraldehyde to produce glyceric acid (Fig.S16b), but this barrier (92 kJ/mol) is much higher than the barrier facilitated by surface O_3 site (27 kJ/mol, presented in Fig.6 of the main text) and therefore is unlikely to be preferred.

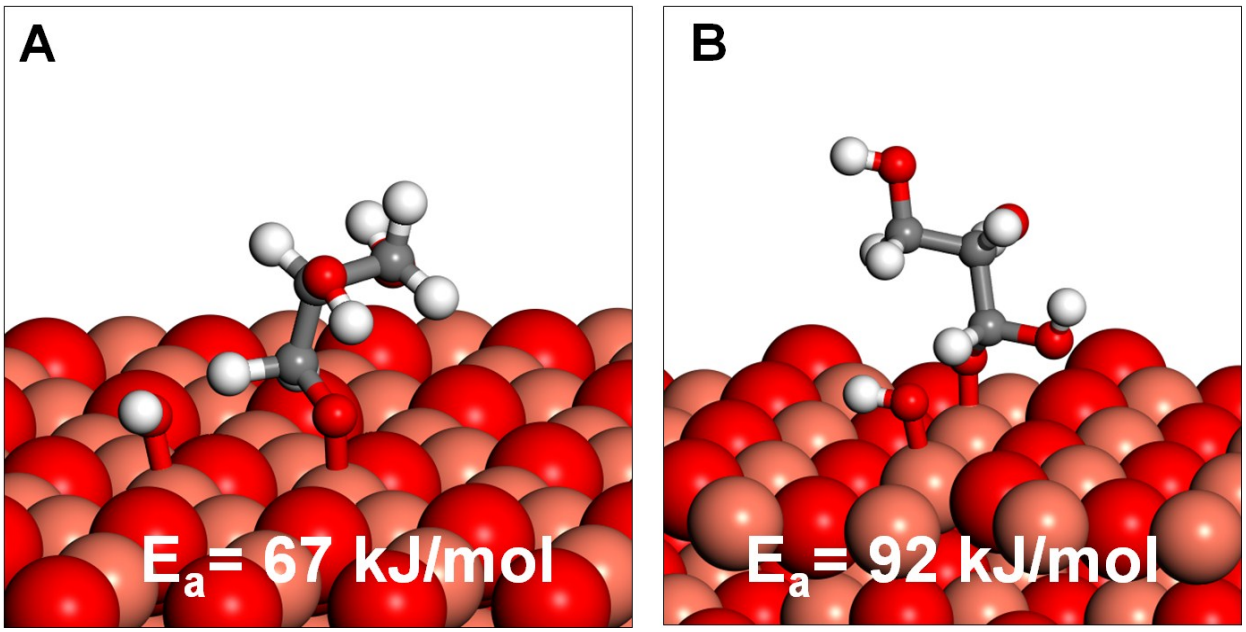

Figure S16. Transition state for surface OH assited in a) C-H activation forming glyceraldehyde and b) H-abstraction forming glyceric acid

15. Compensation of CuO(111) surface by H_2O_2

During the reaction, the lattice Oxygen could be consumed by incorporating itself into the acids generated during the oxidation reaction. This results in the reduction of CuO. The presence of H_2O_2 could provide oxygen to compensate the oxygen vacancies created on the partially reduced CuO (called Cu_nO_{n-1}) to convert it either to Hydrogenated CuO (with H atom adorbs on the surface, called Cu_nO_n-H) or the original CuO (called Cu_nO_n) via the reaction:

$$Cu_nO_{n-1} + 0.5H_2O_2 \rightarrow Cu_nO_n—H \qquad (2)$$

$$Cu_nO_{n-1} + H_2O_2 \rightarrow Cu_nO_n + H_2O \qquad (3)$$

The structures are illustrated in Figure S17. The Gibbs free energy for reactions (2) and (3) are computed at T=80°C (reaction temperature) in a same procedure as was described in Section 11 of the Supporting Information. The results and discussion are presented in the main text.

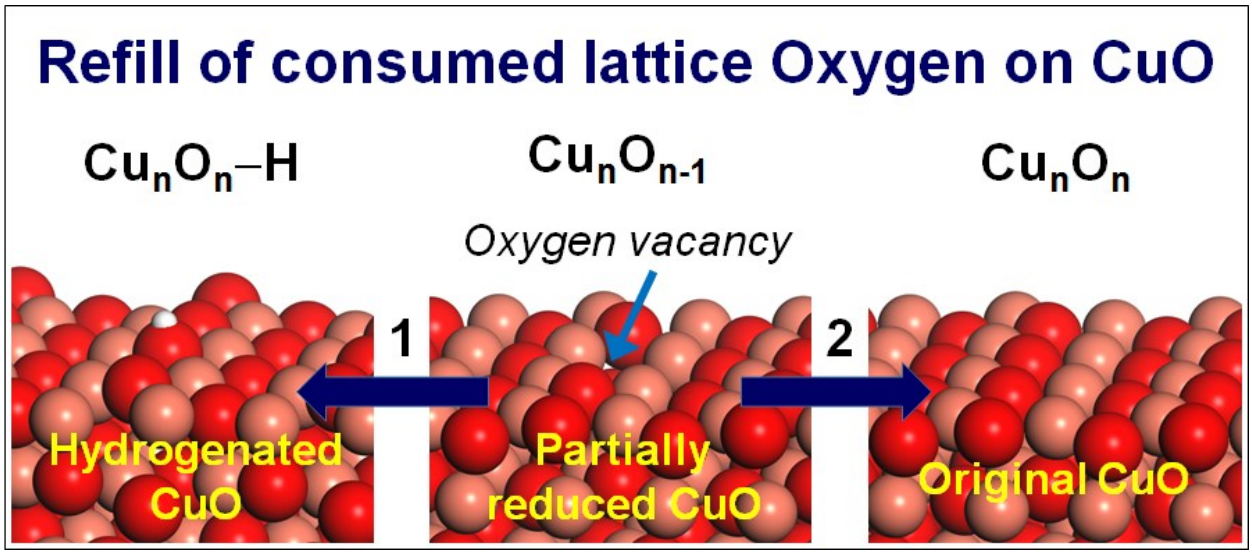

Figure S17. The refill of consumed lattice oxygen on CuO by H_2O_2

16. Market Value of Oxalic Acid

PRODUCTION VOLUME (MT) [13]

REGION	YEAR (2012-2013)	YEAR (2013-2014)	YEAR (2014-2015)	YEAR (2015-2016)	GRWOTH (PERCENT)
Asia	13959	154074	170060	186046	9.4
Europe	35475	38560	41914	45267	8.0
North America	60	64	70	75	7.2
South America	19	20	22	24	7.2

CONSUMPTION VOLUME (MT) [13]

CONTINENT	QUANTITY (MT)
Asia	4853
Europe	5343
North America	6438
South America	8081
Africa	54
Grand Total	**24769**

REFRENCES

1. Koda, S.; Kimura, T.; Kondo, T.; Mitome, H., A standard method to calibrate sonochemical efficiency of an individual reaction system. *Ultrasonics sonochemistry* **2003,** *10* (3), 149-156.

2. Amaniampong, P. N.; Trinh, Q. T.; Wang, B.; Borgna, A.; Yang, Y.; Mushrif, S. H., Biomass Oxidation: Formyl C□H Bond Activation by the Surface Lattice Oxygen of Regenerative CuO Nanoleaves. *Angewandte Chemie International Edition* **2015,** *54* (31), 8928-8933.

3. Amaniampong, P. N.; Trinh, Q. T.; Li, K.; Mushrif, S. H.; Hao, Y.; Yang, Y., Porous structured CuO-CeO2 nanospheres for the direct oxidation of cellobiose and glucose to gluconic acid. *Catalysis Today* **2017**.

4. Tahir, D.; Tougaard, S., Electronic and optical properties of Cu, CuO and Cu2O studied by electron spectroscopy. *Journal of Physics: Condensed Matter* **2012,** *24* (17), 175002.

5. (a) Kresse, G.; Furthmüller, J., Efficiency of ab-initio total energy calculations for metals and semiconductors using a plane-wave basis set. *Computational Materials Science* **1996,** *6* (1), 15-50; (b) Kresse, G.; Hafner, J., Ab initio molecular dynamics for liquid metals. *Physical Review B* **1993,** *47* (1), 558-561.

6. Blöchl, P. E., Projector augmented-wave method. *Physical Review B* **1994,** *50* (24), 17953-17979.

7. Perdew, J. P.; Burke, K.; Ernzerhof, M., Generalized Gradient Approximation Made Simple. *Physical Review Letters* **1996,** *77* (18), 3865-3868.

8. Dudarev, S. L.; Botton, G. A.; Savrasov, S. Y.; Humphreys, C. J.; Sutton, A. P., Electron-energy-loss spectra and the structural stability of nickel oxide: An LSDA+U study. *Physical Review B* **1998,** *57* (3), 1505-1509.

9. (a) Singuru, R.; Trinh, Q. T.; Banerjee, B.; Govinda Rao, B.; Bai, L.; Bhaumik, A.; Reddy, B. M.; Hirao, H.; Mondal, J., Integrated Experimental and Theoretical Study of Shape-Controlled Catalytic Oxidative Coupling of Aromatic Amines over CuO Nanostructures. *ACS Omega* **2016,** *1* (6), 1121-1138; (b) Varghese, J. J.; Trinh, Q. T.; Mushrif, S. H., Insights into the synergistic role of metal-lattice oxygen site pairs in four-centered C-H bond activation of methane: the case of CuO. *Catalysis Science & Technology* **2016,** *6* (11), 3984-3996.

10. Mishra, A. K.; Roldan, A.; de Leeuw, N. H., CuO Surfaces and CO2 Activation: A Dispersion-Corrected DFT+U Study. *The Journal of Physical Chemistry C* **2016,** *120* (4), 2198-2214.

11. (a) Trinh, Q. T.; Banerjee, A.; Yang, Y.; Mushrif, S. H., Sub-Surface Boron-Doped Copper for Methane Activation and Coupling: First-Principles Investigation of the Structure, Activity, and Selectivity of the Catalyst. *The Journal of Physical Chemistry C* **2017,** *121* (2), 1099-1112; (b) Trinh, Q. T.; Nguyen, A. V.; Huynh, D. C.; Pham, T. H.; Mushrif, S. H., Mechanistic insights into the catalytic elimination of tar and the promotional effect of boron on it: first-principles study using toluene as a model compound. *Catalysis Science & Technology* **2016,** *6* (15), 5871-5883; (c) Trinh, Q. T.; Yang, J.; Lee, J. Y.; Saeys, M., Computational and experimental study of the Volcano behavior of the oxygen reduction activity of PdM@PdPt/C (M=Pt, Ni, Co, Fe, and Cr) core–shell electrocatalysts. *Journal of Catalysis* **2012,** *291*, 26-35.

12. (a) Trinh, Q. T.; Chethana, B. K.; Mushrif, S. H., Adsorption and Reactivity of Cellulosic Aldoses on Transition Metals. *The Journal of Physical Chemistry C* **2015,** *119* (30), 17137-17145; (b) Zope, B. N.; Hibbitts, D. D.; Neurock, M.; Davis, R. J., Reactivity of the Gold/Water Interface During Selective Oxidation Catalysis. *Science* **2010,** *330* (6000), 74-78.

13. Lifescience Intellipedia, Market Research Report on Oxalic acid (accessed on 25 September 2017) http://www.lifescienceintellipedia.com